Chemical Engineering Journal 161 (2010) 136–145

Contents lists available at ScienceDirect

Chemical Engineering Journal

journal homepage: www.elsevier.com/locate/cej

Photocatalytic degradation of phenol by base metal-substituted orthovanadates

Parag A. Deshpande, Giridhar Madras*

Department of Chemical Engineering, Indian Institute of Science, Bangalore 560012, India

ARTICLE INFO

Article history:
Received 22 March 2010
Received in revised form 22 April 2010
Accepted 23 April 2010

Keywords:
Orthovanadates
Base metal substitution
Photocatalytic degradation
Selectivity
Reaction mechanism

ABSTRACT

Base metal (Cr, Mn, Fe, Ni, Cu) substituted $CeVO_4$ compounds were synthesized by the solution combustion technique. These compounds were characterized by X-ray diffraction, X-ray photoelectron spectroscopy, UV–vis spectroscopy, transmission electron microscopy and BET surface area analyzer. The characterization indicated that the base metals were substituted in the ionic state in all the compounds. These compounds were used for the photocatalytic degradation of phenol and the degradation rates obtained in the presence of these compounds were compared against that obtained with the commercial Degussa P-25 TiO_2 catalyst. Fe and Cr substituted $CeVO_4$ showed photocatalytic activity that was comparable with that of Degussa P-25 TiO_2. The concentration of toxic intermediates was high when the reaction was carried out in presence of Degussa P-25 TiO_2 but it was found to be insignificant when the reaction was carried out in presence of base metal-substituted $CeVO_4$. The effect of % Fe-substitution (varied from 1 to 5 at%) in $CeVO_4$ on the photocatalytic activity was also investigated and it was observed that 1 at% Fe-substituted compound showed the highest activity. A mathematical model describing the kinetics of the photocatalytic degradation of phenol was developed on the basis of the catalyst structure and taking into account the formation of all the possible intermediates. The variation of the concentration of phenol and the intermediates was described by the model and the reaction rate constants were determined.

1. Introduction

Acute exposure of human beings to phenol is lethal owing to the rapid skin absorption and associated chronic effects. Its effects on living tissues include alteration of the metabolism, chromosomal changes, haemotoxicity, reproductive and developmental toxicity, mutagenesis and carcinogenesis [1]. During the degradation of phenol, toxic intermediates like catechol, hydroquinone and pyrogallol are formed, which are also known to have genotoxic and carcinogenic effects [1]. Therefore, the removal of these intermediates is also necessary for complete purification of water.

A number of processes have been used for mineralization of organics present in water. The major processes include catalysis, photocatalysis, sonolysis, ozonolysis, microwave degradation and biodegradation. Photocatalysis is often used for mineralization of organic compounds. Extensive research has been carried out exploring the use of photocatalysts for the degradation of dyes and organics due to stringent environmental norms [2]. Among the different semiconductor materials exhibiting photocatalytic properties, TiO_2 is the most widely used compound for the degradation organics and dyes [2–4].

Changes in the activity of the photocatalyst by transition metal doping have been reported previously by several investigators [2,5–7]. Both enhancement as well as depletion in activity has been observed by metal doping in TiO_2. We have previously reported the detrimental effect of metal doping in combustion synthesized TiO_2 [5,6]. However, enhancement in the activity by doping Fe and Cu in TiO_2 has also been reported [7,8]. Doping of Fe^{3+} ion in TiO_2 has been reported to enhance the photocatalytic degradation of dyes [9–11] and organics [12].

Orthovanadates constitute another class of compounds that may function as photocatalysts for the degradation of pollutants in water. Several methods have been reported for the synthesis of orthovanadates [13,14]. We have previously reported the photocatalytic activity of Li, Ca and Fe-substituted $CeVO_4$ synthesized by solid state synthesis [15], lanthanide molybdovanadates synthesized by solid state synthesis [16], lanthanide orthovanadates synthesized by solid state [17] and microwave synthesis [18], and Pd substituted $CeVO_4$, synthesized by the solution combustion technique [19]. Combustion synthesis, which is used in this study, leads to the formation of nanocrystallites with high surface area and therefore, the compounds are expected to show high photocatalytic activity [20,21].

* Corresponding author. Tel.: +91 80 2293 2321; fax: +91 80 2360 0683.
E-mail addresses: giridhar@chemeng.iisc.ernet.in, giridharmadras@gmail.com (G. Madras).

1385-8947/$ – see front matter © 2010 Elsevier B.V. All rights reserved.
doi:10.1016/j.cej.2010.04.046

This study aims at the synthesis of a series of base metal-substituted nanocrystalline $CeVO_4$ compounds and determines their photocatalytic activity towards phenol degradation. Except for Fe-substituted $CeVO_4$, which has been synthesized using solid state techniques [17] and by the solution combustion synthesis [15,22], there have been no reports of the synthesis of the other base metal-substituted $CeVO_4$ compounds by any of the methods. The photocatalytic activity of vanadates is less explored but the structural investigations suggest that the compounds exhibit potential characteristics as photocatalysts. The compounds show apparent and false band gaps due to the presence of oxygen ion vacancies with states close to the conduction band [23]. The contributions to electron-hole formation and recombination processes have been attributed mainly due to O 2p orbitals. In such cases, doping, which can further create vacancies, is expected to play a vital role in governing the photocatalytic activity of the vanadates. We report enhanced photocatalytic activity of $CeVO_4$, substituted with Cr, Mn, Fe, Ni and Cu ions. We present a new kinetic model for phenol degradation, present the kinetics of the photodegradation and compare the activity of the catalysts using the estimated rate parameters. We also show that the activity of these catalysts is comparable to that of commercial titania and that the formation of toxic intermediates in presence of these catalysts is negligible.

2. Experimental

2.1. Catalyst synthesis

For the combustion synthesis of $CeVO_4$, ceric ammonium nitrate ($(NH_4)_2Ce(NO_3)_6$, Merck, India), ammonium metavanadate (NH_4VO_3, Rolex, India) and oxalyldihydrazide ($C_2H_6N_4O_2$, Alfa Aesar, India) were taken in stoichiometric amounts. A small amount of water and a few drops of HNO_3 (Merck, India) were added to obtain a clear solution. The solution was heated in a preheated muffle furnace at 350 °C. The product of combustion was removed and finely ground. The fine powder was used as the photocatalyst. For substituting Cr, Mn, Fe, Ni and Cu ions, chromium (III) nitrate nonahydrate ($Cr(NO_3)_3{\cdot}9H_2O$), manganese(II) nitrate hexahydrate ($Mn(NO_3)_2{\cdot}6H_2O$), ferric (III) nitrate nonahydrate ($Fe(NO_3)_3{\cdot}9H_2O$), nickel (II) nitrate hexahydrate ($Ni(NO_3)_2{\cdot}6H_2O$) and copper (III) nitrate trihydrate ($Cu(NO_3)_2{\cdot}3H_2O$) (all from S. D. Fine Chem, India), respectively, were added to the solution and the combustion procedure was repeated. Compounds of different colors were obtained showing the substitution of different ions in the crystal. Further details on the solution combustion synthesis of $CeVO_4$ can be found elsewhere [19].

2.2. Catalyst characterization

All the compounds were characterized by powder X-ray diffraction (XRD), X-ray photoelectron spectroscopy (XPS), UV–vis spectroscopy, transmission electron microscopy (TEM) and BET surface area analyzer. The XRD patterns of the compounds were recorded on Phillips X'pert diffractometer using CuKα radiations. The XPS were recorded on Thermo Fisher Scientific Multilab 2000 instrument with AlKα radiations (1486.6 eV). The spectra were calibrated using C1s binding energy at 284.5 eV. The UV–vis spectra were recorded on Lambda 32, PerkinElmer spectrophotometer. The TEM analysis was carried out on JEOL 200CX TEM machine. The surface areas of the compounds were determined using NOVA-1000, Quantachrome apparatus with nitrogen as adsorbent.

2.3. Photocatalytic setup and experiments

The setup for photocatalytic experiments consisted of a quartz tube and a jacketed glass vessel. The quartz tube was placed inside the jacket and the solution of phenol in water was in the annulus along with the catalyst. A high pressure mercury lamp (Philips, India) was used as a source of UV radiation and was placed inside the quartz tube. The lamp radiated predominantly 365 nm radiations with a flux of 25 W/m^2. Cold water was circulated by a pump through the jacketed vessel to remove the heat generated by the UV lamp and to maintain a constant temperature around 25 °C. The solution in the reactor was continuously stirred using a magnetic stirrer. A catalyst concentration of 1 g/l was maintained in all the experiments. Further details on the experimental setup are provided elsewhere [24].

Samples were taken at regular intervals and centrifuged to separate the catalyst particles. The supernatant clear liquid was taken and diluted with distilled water for the analysis of phenol. The concentration of phenol was determined using high pressure liquid chromatography with a UV detector. Standard solutions of known concentrations of phenol, catechol, hydroquinone, resorcinol and pyrogallol were prepared and injected into the column. The peaks corresponding to each of the compounds were obtained. The residence time of each of the component was found to be different. The separation of phenol [25] from its possible intermediates was carried out in a C18 column (Waters, USA) with an eluent composition of acetic acid:acetonitrile:water = 2.4:15:87.6. The flow rate of the eluent was maintained at 1 ml/min. The separated compounds were detected using a UV detector (Waters, USA) at 270 nm. The calibration plots of phenol and the intermediates in the concentration range of 1–50 ppm were found to be linear. The components of the mixture were determined on the basis of their retention times and were quantified using the calibration plots. To further verify the intermediates, the samples were injected into LC–MS (Waters 3100 mass detector). It was confirmed (by matching the spectra) that the intermediates observed in the samples were catechol, hydroquinone and pyrogallol. Further, TOC analysis of the solution was conducted by a TOC analyzer (Shimadzu TOC-V CSN). All the experiments were repeated three times and the standard deviation in the concentration reported was less than 4%. Similar to our previous studies [26], the catalytic activity of the compound was tested for several cycles. For this purpose, after the reaction, the catalyst was removed, washed with water and the catalyst was reused. This cycle was repeated seven times and there was no appreciable decrease in the rate of conversion of phenol.

3. Results and discussion

3.1. Structural analysis

3.1.1. Powder X-ray diffraction

The XRD patterns of all the compounds were recorded to determine the crystal structure of the compound and to find the lattice position of the dopants in the crystals. XRD patterns of $CeVO_4$ and metal substituted $CeVO_4$ are shown in Fig. 1. The diffraction lines in the XRD of the compounds were indexed to the tetragonal zircon structure with a space group of $I4_1/amd$. No lines corresponding to the metal in zero state were observed for 2 at% compounds. This showed the substitution of the metal in the lattice for Ce^{3+} ions. The patterns of all the compounds resembled and the parent zircon structure of $CeVO_4$ was retained after substitution. Fe-substitution in $CeVO_4$ was increased from 1 to 10 at%. Up to 5 at% Fe-substitution in the lattice, the crystal structure remained unchanged and no additional peaks corresponding to metal or metal oxides were present. However, for 10 at% substitution of Fe, small impurity peaks could be observed corresponding to the oxide phases. This indicated incomplete substitution of the metal in the lattice [22]. Therefore, experiments were not conducted with $Ce_{0.9}Fe_{0.1}VO_4$. Further details can be found elsewhere [19].

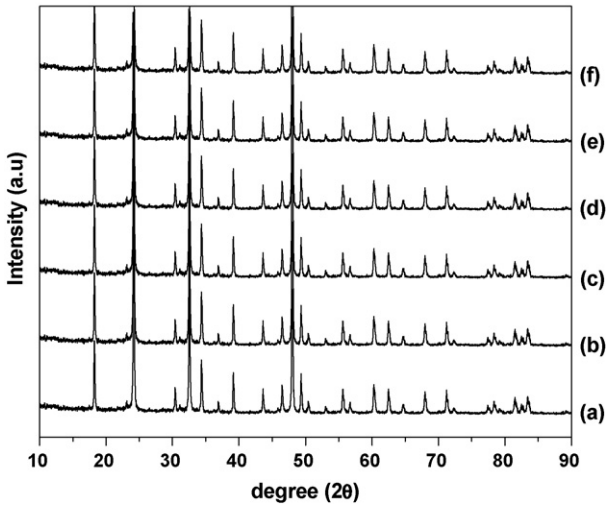

Fig. 1. X-ray diffraction patterns of (a) $CeVO_4$, (b) $Ce_{0.98}Cr_{0.02}VO_4$, (c) $Ce_{0.98}Mn_{0.02}VO_4$, (d) $Ce_{0.98}Fe_{0.02}VO_4$, (e) $Ce_{0.98}Ni_{0.02}VO_4$, and (f) $Ce_{0.98}Cu_{0.02}VO_4$.

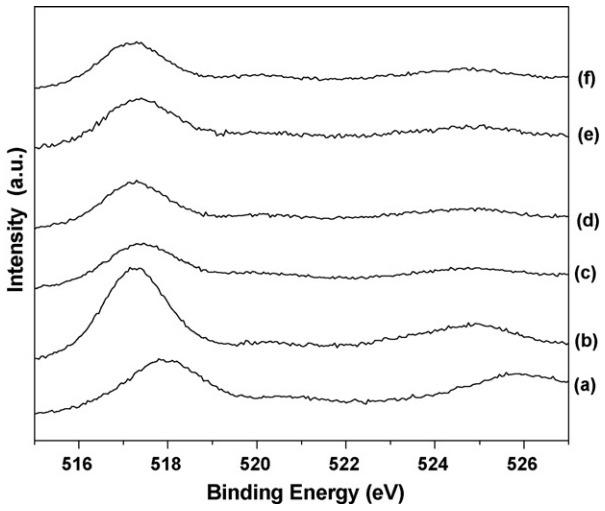

Fig. 3. X-ray photoelectron spectra of V2p in (a) $CeVO_4$, (b) $Ce_{0.98}Cr_{0.02}VO_4$, (c) $Ce_{0.98}Mn_{0.02}VO_4$, (d) $Ce_{0.98}Fe_{0.02}VO_4$, (e) $Ce_{0.98}Ni_{0.02}VO_4$, and (f) $Ce_{0.98}Cu_{0.02}VO_4$.

3.1.2. X-ray photoelectron spectroscopy

The core level XPS of all the compounds were recorded. Fig. 2 shows the Ce3d spectra for unsubstituted and base metal-substituted compounds. All the spectra showed the reduced Ce state. Therefore, in all the compounds, Ce was present in +3 state and the characteristic satellite peaks could be clearly observed. Similarly, from the core level V2p spectra (Fig. 3), V was found to be in +5 state. A small shift in the binding energies was observed for metal-ion substituted compounds. The shift in the binding energies was small indicating that a complete change in the oxidation state of the element did not take place in compound. However, due to the substitution of metal ion in the lattice, differential bond length formation is possible and this may result in shifts in the binding energy in the XPS.

The binding energy of Cr in Cr_2O_3 is 576.2 eV while it is 574.1 eV for metallic Cr [27]. Therefore, the XPS of Cr2p in the compounds (Fig. 4(a)) showed the presence of Cr^{3+} ions. Similarly, for all the other compounds, the metals were present in ionic form. Mn was found to be in +4 state, Ni in +3 state, and Cu in +2 state (Fig. 4(b–d)) as confirmed from the reported values of the binding energies [28]. For the metal to be present in the lattice site substituting the atoms in the parent compound, the ionic nature has to be maintained to satisfy the electrostatic neutrality of the compound. Therefore, from the XPS of the metals in the compounds, it can be deduced that the metals were substituted in the lattice in ionic form. Fe was substituted in different atom percentage up to 10%. Complete substitution up to 5 at% took place and in all the compounds, Fe was present in ionic state. From the XPS, Fe was found to be in mixed oxidation states of +2 and +3 states [22]. In 1% Fe-substituted compound, Fe was present in +2 state. The amount of +3 state increased with increasing substitution and the splitted peaks became clear at higher substitutions. The Fe spectra were decomposed into the various components corresponding to the different oxidation state such that the resultant intensity of the individual spectra matched with the combined intensity. The areas under the individual peaks were calculated to determine the relative contribution of the different states. The amount of Fe^{3+} in 2% and 5% Fe-substituted compound was 20% and 36%, respectively.

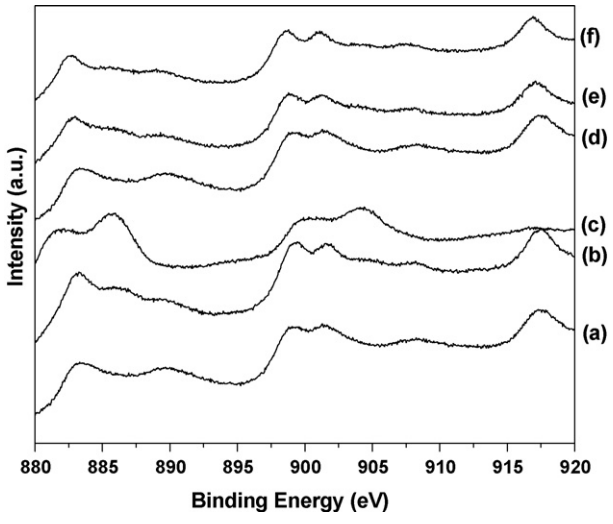

Fig. 2. X-ray photoelectron spectra of Ce3d in (a) $CeVO_4$, (b) $Ce_{0.98}Cr_{0.02}VO_4$, (c) $Ce_{0.98}Mn_{0.02}VO_4$, (d) $Ce_{0.98}Fe_{0.02}VO_4$, (e) $Ce_{0.98}Ni_{0.02}VO_4$, and (f) $Ce_{0.98}Cu_{0.02}VO_4$.

3.1.3. UV–vis spectroscopy

The diffuse reflectance spectra of all the compounds were recorded to determine the band gap of the compounds. Fig. 5(a) shows the spectra for unsubstituted and base- metal substituted $CeVO_4$ and Fig. 5(b) shows the spectra for Fe-substituted $CeVO_4$ with different amounts of Fe-substitution. The band gaps (Table 1) were calculated using the Kubelka–Munk method and the band gap for all the compounds was in the range of 2.00–2.25 eV. These values are not only lower than that for the commercial Degussa P-25 catalyst, having a band gap of 3.2 eV, but also lower than those of the other semiconductors like WO_3 (2.8 eV), $SrTiO_3$ (3.2 eV), α-Fe_2O_3 (3.1 eV), ZnO (3.2 eV) and ZnS (3.6 eV) that are used as photocatalysts [2].

No correlation could be established between the identity of the metal and the band gap. The band gaps were similar for the unsubstituted and for all 2 at% metal-substituted compounds. However, Fe-substituted compounds showed a reduction in band gap from 2.11 to 2.08 eV as the Fe content in the catalyst increased from 2% to 5% due to the increase in the electron density and mobility in the conduction band.

3.1.4. Transmission electron microscopy

The TEM images and electron diffraction patterns of the compounds were recorded. Fig. 6(a and b) shows the TEM images of Ni and Fe-substituted $CeVO_4$, respectively and the diffraction pattern is shown in Fig. 6(c). It is clear from the images that the

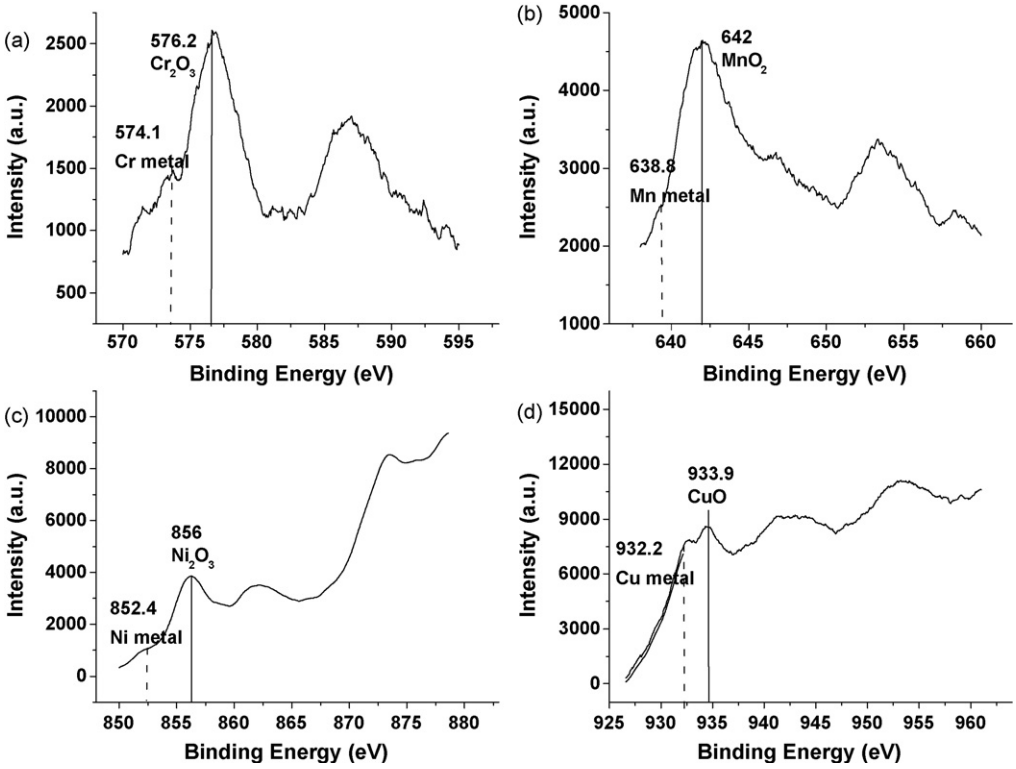

Fig. 4. X-ray photoelectron spectra of (a) Cr2p, (b) Mn2p, (c) Ni2p, and (d) Cu2p in substituted $CeVO_4$.

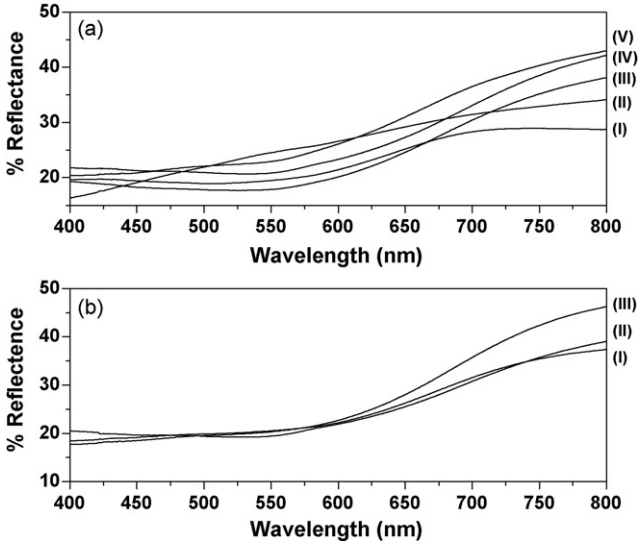

Fig. 5. Diffuse reflectance spectra of (Ia) $CeVO_4$, (Ib) $Ce_{0.98}Cr_{0.02}VO_4$, (Ic) $Ce_{0.98}Mn_{0.02}VO_4$, (Id) $Ce_{0.98}Ni_{0.02}VO_4$, (Ie) $Ce_{0.98}Cu_{0.02}VO_4$, (IIa) $Ce_{0.99}Fe_{0.01}VO_4$, (IIb) $Ce_{0.98}Fe_{0.02}VO_4$, (IIc) $Ce_{0.95}Fe_{0.05}VO_4$.

compounds were nanocrystalline and particles were in the size range of 10–15 nm.

3.1.5. BET surface area

The surface area of the combustion synthesized $CeVO_4$ was found to be 22 m^2/g. The surface areas of all the compounds with 2% base metal substitution were similar to that of $CeVO_4$ and were in the range of 21–22 m^2/g. 1% and 5% Fe-substituted compound had a surface area of 22 and 14 m^2/g, respectively.

Table 1
Band gap of the different base metal substituted compounds.

Compound	Band gap (eV)
$CeVO_4$	2.11
$Ce_{0.98}Cr_{0.02}VO_4$	2.10
$Ce_{0.98}Mn_{0.02}VO_4$	2.13
$Ce_{0.98}Ni_{0.02}VO_4$	2.24
$Ce_{0.98}Cu_{0.02}VO_4$	2.13
$Ce_{0.99}Fe_{0.01}VO_4$	2.12
$Ce_{0.98}Fe_{0.02}VO_4$	2.11
$Ce_{0.95}Fe_{0.05}VO_4$	2.08

3.2. Model for phenol degradation

The degradation of phenol in an aqueous solution involves the hydroxylation of phenol to give intermediate hydroxylated products and the subsequent conversion of these products to CO_2 and H_2O. Under the mild oxidizing conditions provided by H_2O, direct conversion to CO_2 and H_2O is not probable. But water can indeed take part in the reaction along with the dissolved oxygen present in the medium to yield hydroxylated and the final products. Fig. 7 gives a schematic of all the possible pathways that are possible for the degradation of phenol. The intermediates obtained during the degradation of phenol depend upon the method used for degradation. In a recent study, Velasco et al. report the presence of hydroquinone and p-benzoquinone during the photocatalytic degradation of phenol using carbon/titania composite [29]. Intermediates like catechol, hydroquinone, resorcinol, p-benzoquinone and o-benzoquinone have been reported for the degradation of phenol using Fenton's reagent [30]. Hanna et al. have observed only non-aromatic intermediates when the degradation was carried out with Fe(II)-Fe(III) green rust [31]. We have previously reported the photocatalytic activity of Degussa P-25 and combustion synthesized TiO_2 for the degradation of phenol [25]. Catechol and hydroquinone were observed when the reaction was carried

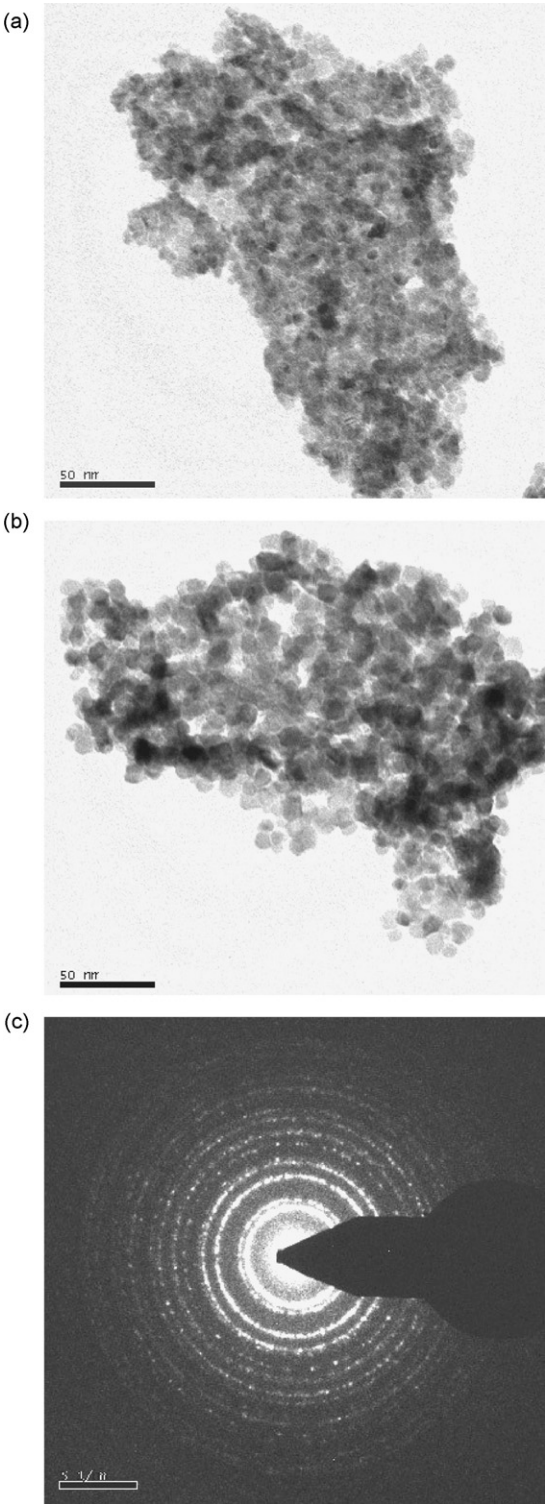

Fig. 6. TEM image of (a) $Ce_{0.98}Ni_{0.02}VO_4$, (b) $Ce_{0.99}Fe_{0.01}VO_4$, and (c) electron diffraction pattern of $Ce_{0.98}Ni_{0.02}VO_4$.

out with commercial Degussa P-25 catalyst. In this study also, we have mainly observed two intermediates over the commercial Degussa P-25 catalyst viz. catechol and hydroquinone. Traces of pyrogallol (<2 ppm) were also detected. However, no intermediates were observed when the degradation of phenol was carried out in presence of the combustion synthesized compound. The absence of intermediates during the reaction in the presence of combustion synthesized compounds is due to the faster rate

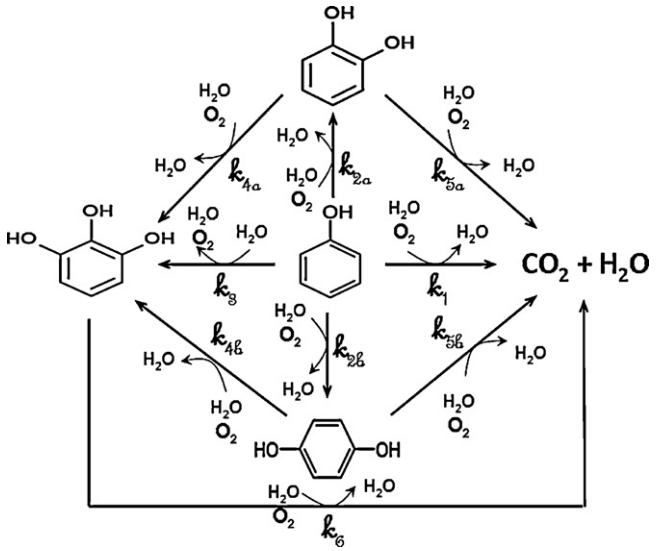

Fig. 7. A schematic of the reaction network for phenol degradation via the different intermediates.

of secondary hydroxylation as compared to the rate of primary hydroxylation.

On the basis of the above arguments, we propose the following set of surface processes taking place during the photocatalysis

$$M/CeVO_4 \overset{+h\nu/-\Delta}{\longleftrightarrow} h^+_{VB} + e^-_{CB} \quad (1)$$

$$Ph + S \leftrightarrow Ph\text{–}S \quad (2)$$

$$H_2O + \text{“v″} \rightarrow H_2\text{“O″} \quad (3)$$

$$O_2 + \text{“v″} \rightarrow \text{“}O_2\text{″} \quad (4)$$

$$H_2\text{“O”} + h^+_{VB} \rightarrow OH^\bullet + H^+ + \text{“v”} \quad (5)$$

$$\text{“}O_2\text{”} + e^-_{CB} \rightarrow \text{“}O_2{}^-\text{”} \quad (6)$$

$$\text{“}O_2{}^-\text{″} + H^+ \rightarrow OH^\bullet + \text{“O″} \quad (7)$$

$$Ph\text{–}S + OH^\bullet \rightarrow I_1(OH^\bullet) \quad (8)$$

$$I_1(OH^\bullet) + OH^\bullet \rightarrow I_2(OH^\bullet) \quad (9)$$

$$I_2(OH^\bullet) \rightarrow ORP + S \quad (10)$$

$$Ph\text{–}S + \text{“O″} \rightarrow ORP + \text{“v″} + S \quad (11)$$

The above set of surface processes accounts for all the experimental observations. Eq. (1) shows the formation of an electron-hole pair in the catalyst by absorption of photons and the recombination releasing heat. The reversible adsorption of phenol over the catalyst surface is given by Eq. (2). The involvement of oxide ion vacancies for both photocatalytic as well as non-photocatalytic reactions have been established in our previous studies [32,33]. The adsorbed phenol is denoted as Ph–S. All the reactions are assumed to take place only over the surface of the catalyst and not in the bulk solution. Therefore, for the reaction, the interaction of the energy source (ultraviolet radiation in the present case), catalyst site and the substrate is necessary. This takes place over the surface of the catalyst. H_2O and O_2 from the medium are adsorbed over the oxide ion vacancies to form the intermediate adsorbed species, given by Eqs. (3) and (4). The holes react with intermediate H_2 “O” species to give active hydroxyl radicals. Similarly, electrons attack the intermediate “O_2” to give the intermediate “$O_2{}^-$” species. The interaction of a proton with “$O_2{}^-$” gives rise to more hydroxyl radicals and intermediate “O” species adsorbed over the support. All these steps are shown by Eqs. (5)–(7).

The involvement of hydroxyl radicals and oxygen has been reported for photochemical organic reactions [2,34–37]. Eqs. (5) and (7) give the formation of hydroxyl radical in solution from H_2O and dissolved O_2. Hoffmann et al. [2] give a detailed mechanism of the hydroxyl radical formation in the aqueous medium involving electron-hole pair generation, electron abstraction by O_2 to give O_2^-, interaction of H_2O with O_2^-, formation of OH^- and subsequent formation of hydroxyl radicals. The reaction of hydroxyl radicals results in the formation of single-hydroxy and double-hydroxy products. These represent catechol, hydoquinone and pyrogallol in the present study and are given by Eqs. (8) and (9). $I_1(OH^\bullet)$ represents a single hydroxylated product whereas $I_2(OH^\bullet)$ represents a double hydroxylated product. However, since the notations do not represent any particular intermediate, Eq. (6) can also represent a reaction yielding the double hydroxylated product. Therefore, Eqs. (8) and (9) satisfy both the conditions of sequential as well as parallel formation of the hydroxylated products. ORP in Eqs. (10) and (11) refers to open ring products, mainly CO_2 and H_2O. ORP desorb to give the catalytically active surface for further reaction. To account for the direct mineralization of phenol to CO_2 and H_2O, Eq. (11) has been proposed. The adsorbed phenol can react with the intermediate oxygen species to give the end products. It is to be noted that the reaction sequence given by Eqs. (1)–(11) form a closed sequence in which all the intermediates are consumed in the subsequent steps. Only Eqs. (8) and (11) form a set of parallel reactions involving adsorbed phenol. Depending upon the relative rates of the two reactions, the depletion of the intermediates takes place and one observes different intermediates with different concentrations.

The rate expression obtained from the set of Eqs. (1)–(11) gives the Langmuir–Hinshelwood type kinetics. The details of the derivation can be found in the Appendix A. It has been assumed that throughout the course of reaction, the flux received by the solution remains constant and the charge recombination processes are much faster than the electron-hole trapping [38,39]. This condition can be represented as

$$k_{-10}[h_{VB}^+]^2 \gg k_{14}\theta_{H_2\text{“}O\text{”}}[h_{VB}^+] + k_{15}\theta_{\text{“}O_2\text{”}}[h_{VB}^+] \quad (12)$$

where, h_{VB}^+ represents the concentration of holes, θ represents the fraction of the total sites covered by the respective species (given as subscript) and k represents the reaction rate constant of the corresponding step. The solution of the various balance equations with the respective elementary rate expressions gives the rate of consumption of phenol as

$$r = \frac{\alpha[\text{Ph}]}{1+\beta[\text{Ph}]} \quad (13)$$

where,

$$\alpha = \frac{(K_{12}+K_{13})k_{20}}{K_{13}} \quad (14)$$

and,

$$\beta = \frac{1+(K_{12}/k_{14}K_C)+(K_{13}/k_{15}K_C)+(K_{13}/k_{20})}{(K_{13}/k_{20})} \quad (15)$$

Clearly, Eq. (19) is of the form described by the Langmuir–Hinshelwood kinetics.

Hoffmann et al. [2] have discussed the relative order of the time scales involved in the various elementary processes during a photocatalytic reaction. The charge carrier generation is reported to be the fastest with a time scale of the order of femtoseconds. The other processes including charge-carrier trapping and recombination require time of the order of nanoseconds. In the reaction sequence proposed in this study, steps (4) and (11) are the key rate determining steps. The rate parameters corresponding to these steps appear prominently in the rate expression given by Eq. (13).

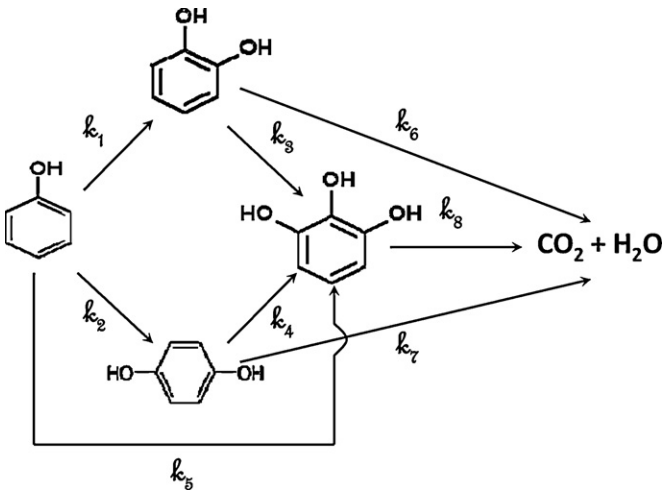

Fig. 8. A schematic of the reduced reaction network for phenol degradation considering primary and secondary hydroxylation processes only.

Therefore, we analyze the effect of these two parameters on the kinetics of the reaction. If $K_{13} \ll k_{20}$, r becomes constant which is not a possible case. However, when $K_{13} \gg k_{20}$, β has a value of the order of 1 and for very small initial concentrations, Eq. (13) can be approximated as

$$r = k[\text{Ph}] \quad (16)$$

where, α has been replaced by k and Eq. (16) gives the degradation kinetics, which is first order in phenol concentration. The above equation is applicable for the current study as the maximum initial concentration of phenol was 1 mmol/l. The same has been established by Rauf and Ashraf [40] and our previous studies [26,41] for the photocatalytic degradation of dyes.

In case of degradation of phenol in presence of Degussa P-25, intermediates are formed, which remain in the solution. Therefore, the kinetics for the formation and consumption of these intermediates needs to be developed. On the basis of the previous arguments regarding the detection of the intermediates, we propose a reduced reaction scheme, given in Fig. 8, in accordance with the experimental observations. The scheme shows the consumption of phenol by conversion to hydroxylated products. The conversion of catechol and hydroquinone to pyrogallol is the process of secondary hydroxylation. Direct conversion of all the hydroxylated products to open ring products, CO_2 and H_2O is also shown.

The rate of degradation of phenol is given as the total rate of its conversion to catechol, hydroquinone and pyrogallol. k in Eq. (16) is the effective reaction rate constant and is given as

$$k = k_1 + k_2 + k_5 \quad (17)$$

where, k_1, k_2 and k_5 represent the reaction rate constant for the conversion of phenol to catechol, hydroquinone and pyrogallol, respectively. The concentrations of phenol, catechol and hydroquinone can be written as

$$[\text{Ph}] = [\text{Ph}]_0 \exp(-kt) \quad (18)$$

$$[\text{Cat}] = [\text{Ph}]_0 \frac{k_1}{k_{36}-k}\{\exp(-kt) - \exp(-k_{36}t)\} \quad (19)$$

$$[\text{Hq}] = [\text{Ph}]_0 \frac{k_2}{k_{47}-k}\{\exp(-kt) - \exp(-k_{47}t)\} \quad (20)$$

where [Ph], [Cat] and [Hq] represent the concentrations of phenol, catechol and hydroquinone, respectively, $[\text{Ph}]_0$ represents the initial concentration of phenol, $k_{36} = k_3 + k_6$ and $k_{47} = k_4 + k_7$. The detailed derivations of the above expressions can be found in the Appendix A.

3.3. Discussion on experimental results

The photocatalytic degradation of phenol was carried out over commercial Degussa P-25 TiO_2 catalyst and combustion synthesized compounds. The variation of phenol concentration with time with an initial concentration of 50 ppm in presence of 1 g/l of Degussa P-25 for the first 30 min is shown in Fig. 9a. Nearly 50% of phenol was degraded in the first 30 min. Catechol and hydroquinone were the only quantifiable organic compounds detected in the solution apart from the traces of pyrogallol. During the initial reaction time, the concentrations of catechol and hydroquinone were 6 and 10 ppm, respectively (Fig. 9a). Both the intermediates were observed simultaneously over the reaction time and complete degradation of the intermediates did not take place. This showed the presence of a complex series-parallel reaction network for mineralization of phenol through catechol, hydroquinone and pyrogallol.

Fig. 9b shows the variation of phenol conversion with time over unsubstituted and 2% base metal-substituted $CeVO_4$ compounds. It can be seen that the rate of reaction increased on substitution. With $CeVO_4$, nearly 18% degradation occurred in the first 30 min. However, 50–55% degradation of phenol was observed in presence of Cr and Fe-substituted $CeVO_4$, which is comparable to 50% degradation observed over the commercial TiO_2 catalyst (Fig. 9a). Further, the formation of catechol and hydroquinone observed during the degradation of phenol in presence of the combustion synthesized compounds was negligible. With Mn, Fe and Ni substitution, these intermediates could not be detected indicating that the concentration of the intermediates was much lesser than 1 ppm. Traces of catechol with concentration not exceeding 3 ppm were observed with Cr and Cu ion substituted compounds. This was still lower than catechol concentration observed when phenol was degraded in presence of Degussa P-25. The concentration of hydroquinone was lesser than 1 ppm when the experiments were conducted with an initial phenol concentration of 100 ppm. This was also negligible as compared to that observed when the degradation was carried out in the presence of Degussa P-25 (Fig. 9a).

To investigate the effectiveness of the catalyst at long times, the reaction was carried out for 5 h. Nearly 80% phenol was degraded in 5 h (Fig. 10a) when the reaction was carried out in presence of Degussa P-25. The conversion increased with time and no saturation concentration was observed even at the end of 5 h. The intermediates continued to be present and 3 and 8 ppm of catechol and hydroquinone, respectively, were observed in the solution at the end of 5 h of degradation (Fig. 10a). Only 55% degradation of phenol was observed over $CeVO_4$ (Fig. 10b). However, nearly 95% of phenol degraded in presence of Fe-substituted compound and 80% was degraded in presence of Cr and Ni substituted compounds. Clearly, the substitution of a metal ion resulted in enhancement of the activity of the catalyst. Although the surface areas of unsubstituted and 2% base metal substituted compounds were similar, a large difference in the activity of the compounds was observed showing the necessity of the redox couple formation and the metal–support interaction required for the high activity of the catalyst. The mechanism proposed in this study shows the utilization of lattice oxygen and formation of intermediates using the dissolved oxygen and aqueous medium. The reducible nature of cerium oxides results in the creation of oxide ion vacancies and the transition of Ce between 3+ and 4+ states takes place. This further results in the reduction of V^{5+} to V^{4+}. The electron-transfers during $Ce^{3+} \leftrightarrow Ce^{4+}$ and $V^{5+} \leftrightarrow V^{4+}$ aid the photochemical processes taking place during the reaction. Substitution of a metal in ionic form results in enhancement of these redox couples and the activity is increased.

The TOC analysis of the solution, exposed to UV radiation for 5 h, was carried out to confirm the mineralization of phenol during the reaction. It was found that the amount of carbon in the solution on long time exposure corresponded to the amount of unreacted phenol in the solution. This confirmed the conversion of phenol to CO_2 and H_2O at longer times.

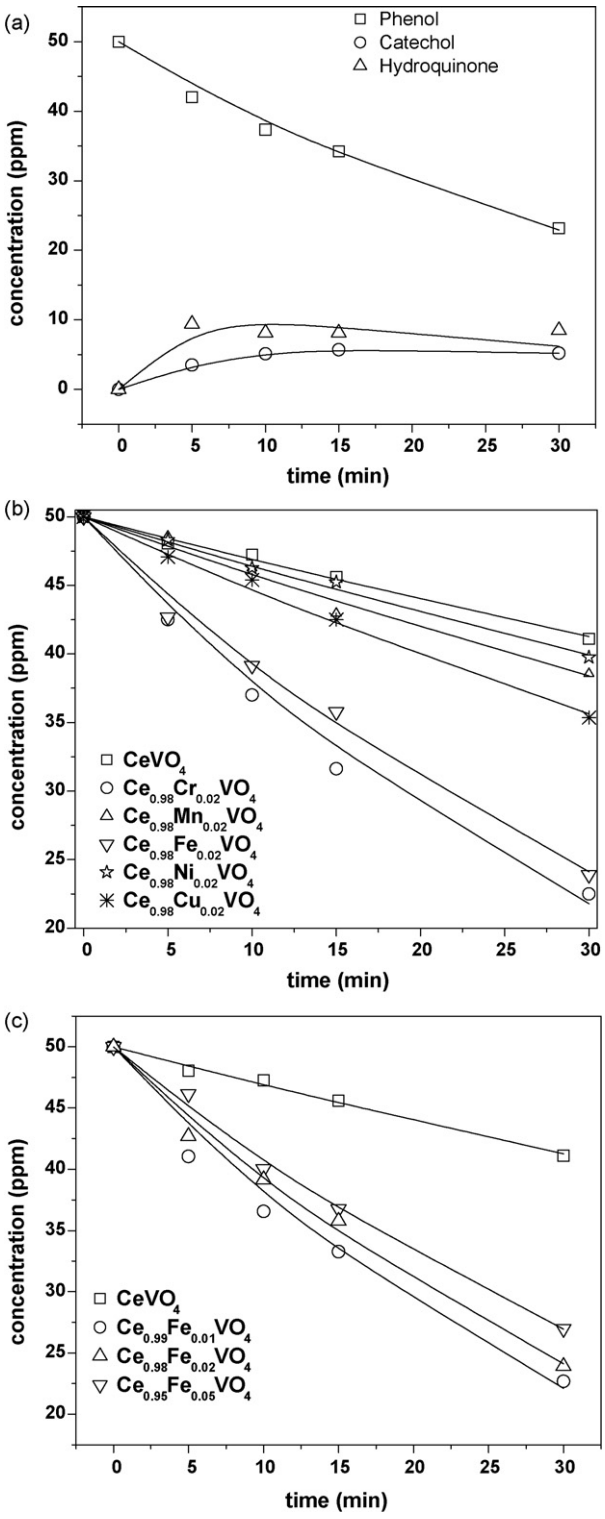

Fig. 9. Variation of phenol concentration with time over (a) commercial Degussa P-25 TiO_2 catalyst, (b) different base metal-substituted compounds, and (c) Fe-substituted $CeVO_4$. The symbols show the experimental data; the lines show the model prediction.

Having established the higher activity of Fe ion substituted compounds as compared to other metal-ion substitutions, the effect of

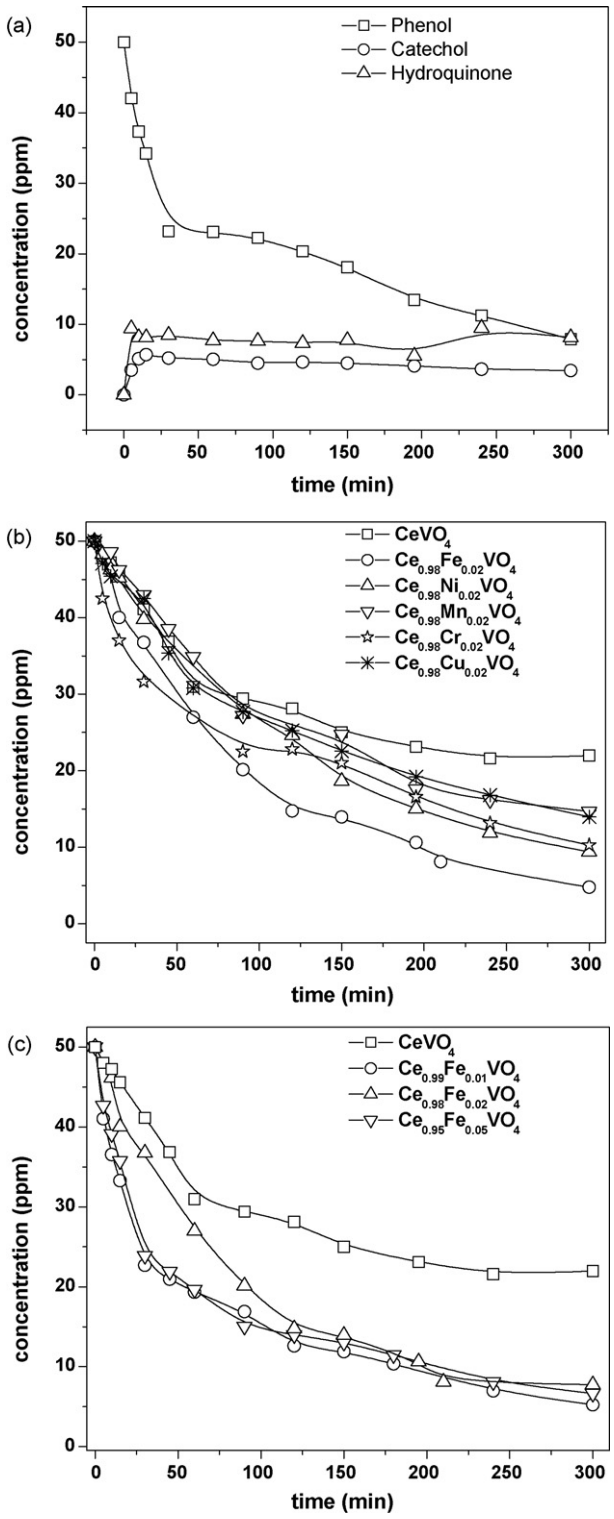

Fig. 10. (a) Variation of the concentration of phenol and the intermediates with time over commercial Degussa P-25 TiO_2 catalyst on exposure to UV radiation for 5 h, (b) variation of phenol concentration with time over different base metal-substituted $CeVO_4$ catalyst on exposure to UV radiation for 5 h, and (c) variation of phenol concentration with time over Fe-substituted $CeVO_4$ catalyst on exposure to UV radiation.

% Fe metal substitution in $CeVO_4$ on the photocatalytic activity was studied by substituting 1%, 2% and 5% Fe in $CeVO_4$. The decrease in concentration of phenol as a function of time is shown in Fig. 10(c). The initial rates and the conversions at the end of 5 h were found to be higher for all the Fe-substituted $CeVO_4$ compounds as compared to the unsubstituted $CeVO_4$. However, with an increase in % substitution, the activity of the compounds decreased. At the end of 5 h of degradation, more than 95% degradation of phenol was observed over 1% Fe-substituted $CeVO_4$ and 1% Fe-substitution showed the higher activity as compared to the activity of unsubstituted and 5% Fe-substituted $CeVO_4$. We have previously observed a decrease in the photocatalytic activity of Fe-substituted $CeVO_4$ for the degradation of dyes [22]. The reason for this can be attributed to the lowering of the surface area and the increase in the Fe^{3+} content in the compound at higher substitutions, thus reducing the redox couples formed.

Table 2
The reaction rate constants for phenol degradation over commercial Degussa P-25 TiO_2 catalyst.

Parameter	Value $\times 10^3$ (min^{-1})
k_1	18.8
k_{36}	99.8
k_2	68.7
k_{47}	274

The variation of the concentrations of phenol, catechol and hydroquinone are given by Eqs. (18)–(20). The rate parameters in Eqs. (18)–(20) were determined by a non-linear regression method based on Levenberg–Marquardt technique. This technique was used to minimize the absolute relative deviation between the experimental data and the model prediction. The experimental data for the variation of the concentrations of phenol and the intermediates along with the model correlation is shown in Fig. 9(a). The various rate constants determined by this technique for the degradation of phenol in presence of Degussa P-25 are given in Table 2. It can be seen that $k_{36} \gg k_1$ and $k_{47} \gg k_2$. This shows that the rate of primary hydroxylation of phenol to catechol or hydroquinone is rate limiting. On the same grounds, the rate of secondary hydroxylation must be even higher as compared to the rate of primary hydroxylation. Therefore, only a small amount of pyrogallol in the solution was detected and mainly catechol and hydroquinone were observed due to relatively lesser consumption rate. Similar trends were observed in our previous studies for the degradation of phenol over combustion synthesized TiO_2, where catechol and hydroquinone were observed as intermediates and secondary hydroxylation was found to be faster than the primary hydroxylation [42].

Fig. 9(b) and (c) shows the variation of phenol concentration with time for different catalysts. The variation of natural log of normalized phenol concentration with time should be linear if the kinetics of degradation of phenol is first order, as given by Eq. (18). Therefore, the logarithm of phenol concentration with time was plotted (Fig. 11(a) and (b)). It can be seen that linear trends were observed for all the compounds indicating that the degradation was first order in phenol concentration. The first order rate constants for phenol degradation in presence of the various catalysts are given in Table 3. The rate constant for phenol degradation in presence of

Table 3
First order reaction rate constants for phenol degradation over the different compounds.

Compound	k (min^{-1}) $\times 10^3$
Degussa P-25	25.0
$CeVO_4$	6.4
$Ce_{0.98}Cr_{0.02}VO_4$	27.7
$Ce_{0.98}Mn_{0.02}VO_4$	8.8
$Ce_{0.98}Ni_{0.02}VO_4$	7.5
$Ce_{0.98}Cu_{0.02}VO_4$	11.3
$Ce_{0.99}Fe_{0.01}VO_4$	27.2
$Ce_{0.98}Fe_{0.02}VO_4$	24.3
$Ce_{0.95}Fe_{0.05}VO_4$	20.6

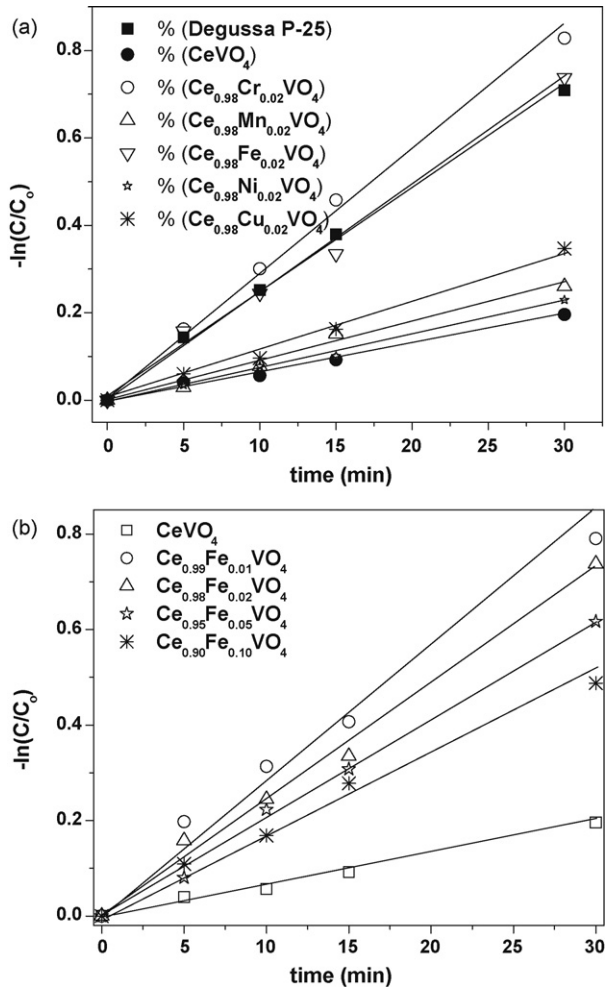

Fig. 11. Variation of natural log of the normalized phenol concentration with time over (a) different base metal-substituted compounds and (b) Fe-substituted $CeVO_4$. The symbols show the experimental data; the lines show the least square linear fit.

the $CeVO_4$ was much lesser than that over the commercial Degussa P-25 TiO_2 catalyst. However, the rate constants for phenol degradation were higher for the substituted compounds and the rate constants observed in presence of Fe and Cr substituted compounds were comparable to that observed with commercial Degussa P-25 TiO_2 catalyst. But the most important advantage of these combustion synthesized compounds is the complete mineralization of phenol with no intermediates remaining in the solution.

4. Conclusions

Photocatalytically active base metal-substituted orthovanadates were synthesized and used for the degradation of phenol. The substitution of base metal ions enhanced the activity of the catalysts. The unsubstituted $CeVO_4$ was found to be inferior while the activity of the base metal-substituted compounds was comparable to the commercial Degussa P-25 TiO_2 catalyst. The toxic intermediates, catachol, hydroquinone and pyrogallol, were observed during phenol degradation over Degussa P-25 TiO_2 whereas their concentrations were negligible when phenol was degraded over the combustion synthesized compounds. Fe-substituted compounds showed high catalytic activity but the activity decreased with an increase in the amount of Fe and 1% Fe-substituted $CeVO_4$ showed the highest photocatalytic activity. A detailed kinetic model for the degradation of phenol was proposed and used to determine the rate constants for degradation.

Acknowledgements

GM gratefully acknowledges Department of Science and Technology for the Swarnajayanti Fellowship. The authors thank Paromita Kundu and Dr. N. Ravishankar of Materials Research Center, IISc for TEM analysis, Dr. Suresh of CGPL, IISc, for surface area measurements and Mr. Khan Mohammad Ammar Raza of NIT Warangal for the initial testing of the photocatalytic activity.

Appendix A. Supplementary data

Supplementary data associated with this article can be found, in the online version, at doi:10.1016/j.cej.2010.04.046.

References

[1] B.J. Dean, Recent findings on the genetic toxicology of benzene, toluene, xylenes and phenols, Mutat. Res. 154 (1985) 153–181.
[2] M.R. Hoffmann, S.T. Martin, W. Choi, D.W. Bahnemannt, Environmental applications of semiconductor photocatalysis, Chem. Rev. 95 (1995) 69–96.
[3] A.L. Linsebigler, G. Lu, J.T. Yates Jr., Photocatalysis on TiO_2 surfaces: principles, mechanisms, and selected results, Chem. Rev. 95 (1995) 735–758.
[4] X. Chen, S.S. Mao, Titanium dioxide nanomaterials: synthesis, properties, modifications and applications, Chem. Rev. 107 (2007) 2891–2959.
[5] K. Nagaveni, M.S. Hegde, G. Madras, Structure and photocatalytic activity of $Ti_{1-x}M_xO_{2\pm d}$ (M = W, V, Ce, Zr, Fe and Cu) synthesized by solution combustion method, J. Phys. Chem. B 108 (2004) 20204–20212.
[6] R. Vinu, G. Madras, Photocatalytic activity of Ag-substituted and impregnated nano-TiO_2, Appl. Catal. A: Gen. 366 (2009) 130–140.
[7] C. Zhang, C. Wang, J. Li, K. Yang, Structural and electronic properties of Fe-doped $BaTiO_3$ and $SrTiO_3$, Chin. Phys. 16 (2007) 1422–1428.
[8] J. Yu, Q. Xiang, M. Zhau, Preparation, characterization and visible-light-driven photocatalytic activity of Fe-doped titania nanorods and first-principles study for electronic structures, Appl. Catal. B: Environ. 90 (2009) 595–602.
[9] L. Sun, J. Li, C.L. Wang, S.F. Li, H.B. Chen, C.J. Lin, An electrochemical strategy of doping Fe^{3+} into TiO_2 nanotube array films for enhancement in photocatalytic activity, Solar Energ. Mater. Solar Cell 93 (2009) 1875–1880.
[10] X. Yang, C. Cao, L. Erickson, K. Hohn, R. Maghirang, K. Klabunde, Photocatalytic degradation of Rhodamine B on C-, S-, N-, and Fe-doped TiO_2 under visible-light irradiation, Appl. Catal. B: Environ. 91 (2009), pp. 657-622.
[11] L. Cui, Y. Wang, M. Niu, G. Chen, Y. Cheng, Synthesis and visible light photocatalysis of Fe-doped TiO_2 mesoporous layers deposited on hollow glass microbeads, J. Solid State Chem. 182 (2009) 2785–2790.
[12] K. Nayeem, F. Ouyang, Preparation of Fe^{3+}-doped TiO_2 nanoparticles and its photocatalytic activity under UV light, Physica B 405 (2009) 221–226.
[13] R.K. Selvan, A. Gedanken, P. Anilkumar, G. Manikandan, C. Karunakaran, Synthesis and characterization of rare earth orthovanadate (RVO_4; R = La, Ce, Nd, Sm, Eu & Gd) nanorods/nanocrystals/nanospindles by a facile sonochemical method and their catalytic properties, J. Clust. Sci. 20 (2009) 291–305.
[14] X. Zhang, Y. Zhanga, X. Quan, S. Chen, Preparation of Ag doped $BiVO_4$ film and its enhanced photoelectrocatalytic (PEC) ability of phenol degradation under visible light, J. Hazard. Mater. 167 (2009) 911–914.
[15] S. Mahapatra, R. Vinu, D. Saha, T.N. Guru Row, G. Madras, Synthesis, characterization and photocatalytic activity of $M_xCe_{1-x}VO_4$ (M = Li, Ca and Fe), Appl. Catal. A: Gen. 391 (2009) 32–41.
[16] S. Mahapatra, G. Madras, T.N. Guru Row, Structure and photocatalytic activity of lanthanide (Ce, Pr, and Nd) molybdovanadates, J. Phys. Chem. C 111 (2007) 6505–6511.
[17] S. Mahapatra, G. Madras, T.N. Guru Row, Synthesis, characterization and photocatalytic activity of lanthanide (Ce, Pr, and Nd) orthovanadates, Ind. Eng. Chem. Res. 46 (2007) 1013–1017.
[18] S. Mahapatra, S.K. Nayak, G. Madras, T.N. Guru Row, Microwave synthesis and photocatalytic activity of nano lanthanide (Ce, Pr, and Nd) orthovanadates, Ind. Eng. Chem. Res. 47 (2008) 6509–6516.
[19] M.B. Bellakki, T. Baidya, C. Shivakumara, N.Y. Vasanthacharya, M.S. Hegde, G. Madras, Synthesis, characterization, redox and photocatalytic properties of $Ce_{1-x}Pd_xVO_4$ ($0 \le x \le 0.1$), Appl. Catal. B: Environ. 84 (2008) 474–481.
[20] M.S. Hegde, G. Madras, K.C. Patil, Noble metal ionic catalysts, Acc. Chem. Res. 42 (2009) 704–712.
[21] K.C. Patil, M.S. Hegde, T. Rattan, S.T. Aruna, Chemistry of Nanocrystalline oxide Materials, first ed., World Scientific, Singapore, 2008.
[22] P.A. Deshpande, G. Madras, Photocatalytic degradation of dyes over combustion-synthezised $Ce_{1-x}Fe_xVO_4$, Chem. Eng. J. 158 (2010) 571–577.
[23] D.P. Butcher, A.A. Gewirth, Photoelectrochemical response of $TlVO_4$ and $InVO_4$:$TlVO_4$ composite, Chem. Mater. 22 (2010) 2555–2562.
[24] R. Vinu, G. Madras, Synthesis and photocatalytic activity of Pd substituted nano-TiO_2, J. Mol. Catal. A: Chem. 291 (2008) 5–11.
[25] G. Sivalingam, M.H. Priya, G. Madras, Effect of substitution on the photocatalytic degradation of phenol using combustion synthesized TiO_2: mechanism and kinetics, Appl. Catal. B: Environ. 51 (2004) 67–76.

[26] K. Nagaveni, G. Sivalingam, M.S. Hegde, G. Madras, Solar photocatalytic degradation of dyes: high activity of combustion synthesized nano TiO_2, Appl. Catal. B: Environ. 48 (2004) 83.
[27] B. Stypula, J. Stoch, The characterization of passive films on chromium electrodes by XPS, Corros. Sci. 36 (1994) 2159–2167.
[28] C.D. Wagner, J.F. Moulder, L.E. Davis, W.M. Riggs, Handbook of X-ray Photoelectron Spectroscopy, PerkinElmer, 1979.
[29] L.F. Velasco, J.B. Parra, C.O. Ania, Role of activated carbon features on the photocatalytic degradation of phenol, Appl. Surf. Sci. (2010), doi:10.1016/j.apsusc.2009.12.113.
[30] M.S. Yalfani, S. Contreras, F. Medina, J. Suegras, Phenol degradation by Fenton's process using catalytic in situ generated hydrogen peroxide, Appl. Catal. B: Environ. 89 (2009) 519–526.
[31] K. Hanna, T. Kone, C. Ruby, Fenton-like oxidation and mineralization of phenol using synthetic Fe(II)-Fe(III) green rusts, Environ. Sci. Pollut. Res. 17 (2010) 124–134.
[32] S. Roy, T. Aarthi, M.S. Hegde, G. Madras, Kinetics of photocatalytic reduction of NO by CO with Pd^{2+}-ion-substituted nano-TiO_2, Ind. Eng. Chem. Res. 46 (2007) 5798–5802.
[33] S. Roy, A. Marimuthu, M.S. Hegde, G. Madras, High rates of NO and N_2O reduction by CO, CO and hydrocarbon oxidation by O_2 over nano crystalline $Ce_{0.98}Pd_{0.02}O_{2-d}$: catalytic and kinetic studies, Appl. Catal. B: Environ. 71 (2007) 23–31.
[34] M.A. Fox, M.T. Dulay, Heterogeneous photocatalysis, Chem. Rev. 93 (1993) 341–357.
[35] T.L. Thompson, J.T. Yates Jr., Surface science studies of the photoactivation of TiO_2—new photochemical processes, Chem. Rev. 106 (2006) 4428–4453.
[36] H. Gerischer, A. Heller, The role of oxygen in photooxidation of organic molecules on semiconductor particles, J. Phys. Chem. 95 (1991) 5261–5267.
[37] H. Gerischer, Photocatalysis in aqueous solution with small TiO_2 particles and the dependence of the quantum yield on particle size and light intensity, Electrochem. Acta 40 (1995) 1277–1281.
[38] G. Rothernberger, J. Moser, M. Graetzel, N. Serpone, D.K. Sharma, Charge carrier trapping and recombination dynamics in small semiconductor particles, J. Am. Chem. Soc. 107 (1985) 8054–8059.
[39] E. Du, Y.X. Zhang, L. Zheng, Photocatalytic degradation of dimethyl phthalate in aqueous TiO_2 suspension: a modified Langmuir–Hinshelwood model, React. Kinet. Catal. Lett. 97 (2009) 83–90.
[40] M.A. Rauf, S.S. Ashraf, Fundamental principles and application of heterogeneous photocatalytic degradation of dyes in solution, Chem. Eng. J. 151 (2009) 10–18.
[41] G. Sivalingam, K. Nagaveni, M.S. Hegde, G. Madras, Photocatalytic degradation of various dyes by combustion synthesized nano anatase TiO_2, Appl. Catal. B: Environ. 45 (2003) 23.
[42] K. Nagaveni, G. Sivalingam, M.S. Hegde, G. Madras, Photocatalytic degradation of organic compounds over combustion-synthesized TiO_2, Environ. Sci. Technol. 38 (2004) 1600.